

## Article

# Role of Cyclic Thermal Shocks on the Physical and Mechanical Responses of White Marble

Yujie Feng <sup>1</sup>, Haijian Su <sup>1,2,\*</sup>, Yinjiang Nie <sup>1</sup> and Honghui Zhao <sup>1,3</sup>

<sup>1</sup> State Key Laboratory for Geomechanics and Deep Underground Engineering, China University of Mining and Technology, Xuzhou 221116, China; yjfeng@cumt.edu.cn (Y.F.); TS20030049A31TM@cumt.edu.cn (Y.N.); hhzhao@cumt.edu.cn (H.Z.)

<sup>2</sup> State Key Laboratory of Coking Coal Exploitation and Comprehensive Utilization, China Pingmei Shenma Group, Pingdingshan 467000, China

<sup>3</sup> East China Environmental Geotechnical Branch, China Petroleum Engineering Construction Company, Qingdao 266000, China

\* Correspondence: hjsu@cumt.edu.cn

**Abstract:** Marble is a common rock used in many buildings for structural or ornamental purposes and is widely distributed in underground engineering projects. The rocks are exposed to high temperatures when a tunnel fire occurs, and they will be rapidly cooled during the rescue process, which has a great impact on the rock performance and the underground engineering stability. Therefore, the role of cyclic thermal shocks on the physical and mechanical properties of marble specimens was systematically investigated. Different cyclic thermal shock treatments ( $T = 25, 200, 400, 600, 800$  °C;  $N = 1, 3, 5, 7, 9$ ) were applied to marble specimens and the changes in mass, volume, density and P-wave velocity were recorded in turn. Then, the thermal conductivity, optical microscopy and uniaxial compression tests were carried out. The results showed that both the cyclic thermal shock numbers ( $N$ ) and the temperature level ( $T$ ) weaken the rock properties. When the temperature of a thermal shock exceeds 600 °C, the mass loss coefficient and porosity of the marble will increase significantly. The most noticeable change in P-wave velocity occurs between 200 and 400 °C, with a 52.98% attenuation. After three thermal shocks, the cyclic thermal shock numbers have little influence on the uniaxial compressive strength and Young's modulus of marble specimens. Shear failure is the principal failure mode in marble specimens that have experienced severe thermal damage (high  $N$  or  $T$ ). The optical microscopic pictures are beneficial for illustrating the thermal cracking mechanism of marble specimens after cyclic thermal shocks.

**Keywords:** marble; cyclic thermal shock; thermal damage; microscopic feature



**Citation:** Feng, Y.; Su, H.; Nie, Y.; Zhao, H. Role of Cyclic Thermal Shocks on the Physical and Mechanical Responses of White Marble. *Machines* **2022**, *10*, 58. <https://doi.org/10.3390/machines10010058>

Academic Editor: Xiaosheng Gao

Received: 1 December 2021

Accepted: 12 January 2022

Published: 13 January 2022

**Publisher's Note:** MDPI stays neutral with regard to jurisdictional claims in published maps and institutional affiliations.



**Copyright:** © 2022 by the authors. Licensee MDPI, Basel, Switzerland. This article is an open access article distributed under the terms and conditions of the Creative Commons Attribution (CC BY) license (<https://creativecommons.org/licenses/by/4.0/>).

## 1. Introduction

To ensure the stability and safety of rock engineering, it is critical to understand the physical and mechanical properties of rock. In practical engineering, rocks tend to be subjected to complex conditions that degrade their rock properties. The degradation of rocks can be attributed to a variety of factors; one that should not be overlooked is temperature. Underground coal gasification (UCG), geothermal energy exploitation, nuclear waste disposal, fire hazards in underground tunnels and the maintenance/restoration of stone-built heritage following fire exposure are among examples of rock engineering applications that involve high temperatures [1–5]. In its natural state, rock material is a typical porous medium with primary microscopic holes and fissures [6,7]. Mineral thermal expansion and reactions would occur in the rocks at elevated temperatures, resulting in the extension of pre-existing micro-cracks and the initiation of new cracks. As a result, physical and mechanical parameters (such as density, P-wave velocity and compressive strength) would vary significantly as temperature rises, as demonstrated experimentally by measurements of rocks after exposure to high temperatures [8–11]. The failure of rock

under the effect of high temperatures and generated stress has developed into one of the primary research topics in the rock mechanics field. In underground engineering involving rock cyclic thermal shock, the change of rock properties after cyclic thermal shock plays a very important role in the stability of underground engineering. For example, the physical and mechanical properties of the rock mass exposed to high temperatures will be affected in a tunnel fire. In the rescue process, cold water is used to artificially cool the high-temperature rocks quickly, and the strength of the tunnel after cyclic thermal shock affects the safe operation of the tunnel [12,13]. In a fire, the temperature of the inner wall of the tunnel can reach as high as 1200 °C [14,15]. Another example is that if the drilling fluid cannot circulate smoothly during the drilling process, the high-speed and continuous friction between the drill bit and the hole wall will increase the temperature of the drilled rock and affect the drillability of the rock. Recently, a new drilling method of heating the rocks around the drill bit to assist drilling was proposed and the temperature encountered may reach 1000 °C [10,16].

Marble rocks are frequently utilized as structural and ornamental construction materials, such as columns, flooring, reliefs and monuments, since they are natural stones with high aesthetic value and workability. It is a noble stone with outstanding beauty and flexibility of manipulation, but it is vulnerable to being subjected to high temperatures, either naturally or artificially [17–21]. In some mountain tunnels, water conservancy and hydropower projects in southwest China, marble is a common rock mass medium [22–24]. For example, marble is widely distributed in the diversion tunnel of Jinping hydropower station, which has the highest head and largest installed scale on the Yalong River [25]. The stability of the diversion tunnel is directly related to the normal operation and safety of the hydropower station because of its large, buried depth, line length and diameter. Once a fire occurs and is not properly handled, it will cause great damage to the stability and economy of the project.

Marble is a fairly simple rock material, which is composed primarily of calcite and dolomite. Thermal stress would be generated at high temperatures due to the differing thermal expansion coefficients of calcite and dolomite [2,26]. Once the induced thermal stress surpasses the cohesiveness threshold, macroscopic changes in the physical and mechanical properties can be noticed. It is well established that the degradation of rocks is mainly dependent on the development of micro-cracks. Anisotropic thermal expansion within rocks results in both thermal gradients and cycling cracks [27]. Thermal gradient cracks are caused by an inhomogeneous temperature field within the rock specimen, whereas thermal cycling cracks are primarily caused by mismatches in the thermal expansion of various minerals. The thermal gradient cracks are not the research object of this work. According to the studies of Li et al. [28] and Zhang et al. [29,30], selecting a low heating rate during the high temperature treatment may minimize the effect of the thermal gradient. In the past few decades, some researchers have studied the effects of thermal damage on the physical and mechanical properties of marble rocks under post-high temperature conditions by laboratory testing [17–19,26,31,32]. For example, Ozguven and Ozelik [31] heated the marble and limestone specimens up to 1000 °C and investigated the effect of the thermal gradient on physical and mechanical properties such as density, porosity, uniaxial compressive strength and tensile strength. Their results demonstrated that the apparent porosity increases with temperature, probably due to capillary cracks caused by heat. Peng et al. [32] performed uniaxial compression tests on coarse marble specimens subjected to high temperatures of 200, 400 and 600 °C and discovered mechanical property degradation laws with temperature. The color changes and ultrasonic responses were also studied. Gautam et al. [26] studied the physical and mechanical properties of thermally treated marble at a temperature range of 25–700 °C and observed that dolomites decompose under thermal stress into calcium and magnesium oxides.

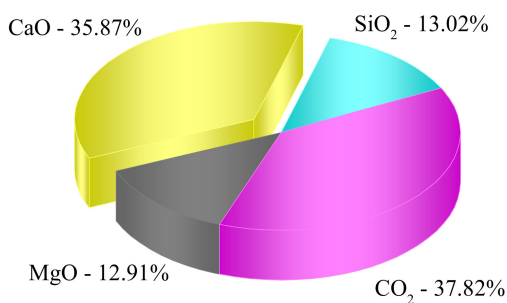
Despite the fact that numerous experimental studies have been conducted to determine the deteriorations in the physical and mechanical properties of marble rocks after high temperature treatment, there is no systematic study on the changes in properties of high-

temperature rock masses after rapid cooling. Rocks are believed to have experienced a thermal shock after being subjected to high temperatures and rapid cooling. In addition, the weakening of rock properties caused by thermal shock is not only due to the change in temperature levels, but also affected by the number of thermal shock cycles. Therefore, different temperature levels (25, 200, 400, 600 and 800 °C) and cyclic thermal shock numbers (1, 3, 5, 7, 9) were chosen in the present study to investigate the role of cyclic thermal shock on the physical, mechanical properties of marble specimens. The thermogravimetry of dolomite and optical microscopy were analyzed to help explain the thermal damage mechanism of marbles.

## 2. Experimental Methodology

### 2.1. Specimens Preparation

The tested white marble block was collected from the Shandong province of China and no visible cracks could be observed on the surface with the naked eye. The average density of tested marble rock is 2.845 g/cm<sup>3</sup> and the average P-wave velocity is 4.98 km/s. From the X-ray fluorescence (XRF) results in Figure 1a, the main chemical compositions of the tested white marble are CaO, CO<sub>2</sub>, SiO<sub>2</sub> and MgO, which, respectively, account for 35.87, 37.82, 13.02 and 12.91%. Some trace chemical components such as Al<sub>2</sub>O<sub>3</sub>, K<sub>2</sub>O and Fe<sub>2</sub>O<sub>3</sub> are not clearly shown in the figure, and their proportions are as follows: 0.37, 0.06 and 0.17%. In addition, the XRD tests demonstrated that dolomite is the principal mineral of the tested marble specimens. As shown in Figure 1b, cylinder specimens with a diameter of 50 mm and a length of 100 mm were drilled from the marble block in an identical direction to reduce the effects of rock heterogeneity. The two end surfaces of the specimens were polished to control the flatness and parallelism within ±0.02 and ±0.05 mm according to the ISRM suggested method [33].



(a)



(b)

**Figure 1.** (a) XRF result of tested marble; (b) Images of tested marble specimens.

### 2.2. Cyclic Thermal Shock Treatment

Rapid cooling of a high-temperature rock specimen to room temperature is regarded as a thermal shock. Figure 2a illustrates the schematic diagram of cyclic thermal shock treatment. One thermal shock cycle involves heating the marble specimens to the set temperature at a rate of 5 °C per minute, maintaining the temperature for 2 h, and then immediately removing them from the muffle furnace and rapidly cooling them to room temperature with water. After the high temperature tests of many scholars [34–36], it is believed that a low heating rate of 5 °C/min can minimize the impact of thermal gradients. Therefore, the effects of temperature and cyclic thermal shock numbers can be focused on in this work. Following each thermal shock treatment, the marble sample was dried for 2 h in an oven at a temperature of 105 °C to remove any remaining moisture before

proceeding to the next thermal shock. In the experiment, five temperature levels were designed ( $T = 25, 200, 400, 600, 800$  °C). At  $T = 200$  and  $400$  °C, the marble specimens all underwent different thermal shock numbers ( $N = 1, 3, 5, 7, 9$ ). While visible pores and macroscopic cracks appeared on the surface of marble specimens following five thermal shock cycles at  $600$  °C and a single thermal shock at  $800$  °C (Figure 2b), no additional cyclic thermal shock treatments were performed on them. Thus, the cyclic thermal shock number ( $N$ ) for  $T = 600$  °C was adjusted to 1, 3 and 5, respectively. Notably, 2–3 specimens were prepared for each condition to obtain the average and eliminate random errors.

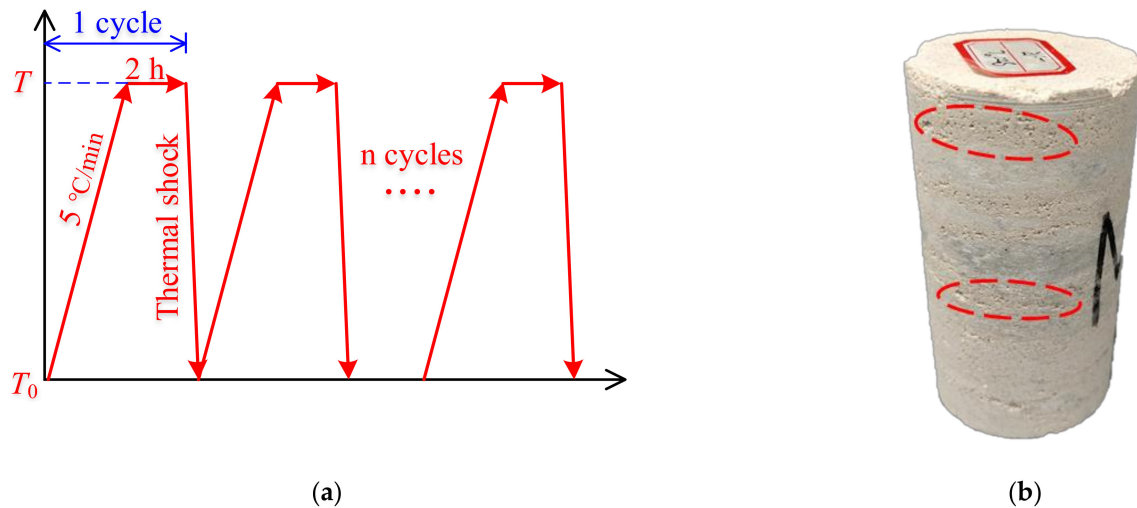


**Figure 2.** (a) Schematic diagram of cyclic thermal shock; (b) Marble specimen underwent thermal shock treatment of  $800$  °C.

### 2.3. Testing Procedures

After cyclic thermal shock treatment, the basic physical properties, including mass, volume, density, P-wave velocity, porosity and thermal conductivity, of the specimens were, respectively, measured. At high temperatures, free water and absorbed water inside rocks escape, and particles may expand to some extent, resulting in mass loss and volume expansion of marble specimens. To better illustrate the variations in mass and volume, mass loss coefficient ( $\gamma$ ) and volume expansion level ( $\eta$ ) are introduced, which can be calculated by the following equations:

$$\gamma = \frac{M_0 - M_n}{M_0} \times 100\% \quad (1)$$

$$\eta = \frac{V_n - V_0}{V_0} \times 100\% \quad (2)$$

where  $M_0$  and  $V_0$  represent the initial mass and volume of specimens prior to cyclic thermal shock treatment, respectively, and  $M_n$  and  $V_n$  represent the ultimate mass and volume of specimens following cyclic thermal shock treatment, respectively. The P-wave velocity was measured using an HC-U81 ultrasonic wave tester, the installation and operation of which are described in Figure 3a. It was calculated as the ratio of the specimen's length to the pulse time that passes through it. To increase the accuracy of the experimental data, Vaseline was chosen as the coupling medium between the specimen and the transducers. Porosity was determined using the BH-1 rock porosity test system (Figure 3b), which operates on the following principle:

$$\varphi = \frac{M_{\text{sat}} - M_{\text{d}}}{V_n \times \rho_w} \times 100\% \quad (3)$$

where  $M_{\text{sat}}$  and  $M_{\text{d}}$  denote the mass of fully saturated specimens and dried specimens, respectively, and  $\rho_w$  denotes the density of pure water. Thermal conductivity was measured

using a Hot Disk thermal constants analyzer, as illustrated in Figure 3c. Two specimens were needed for each test, and a small amount of force along the axial direction of specimens was required in order to make the sensor of the analyzer, which is composed of thin nickel foils, come into full contact with them.

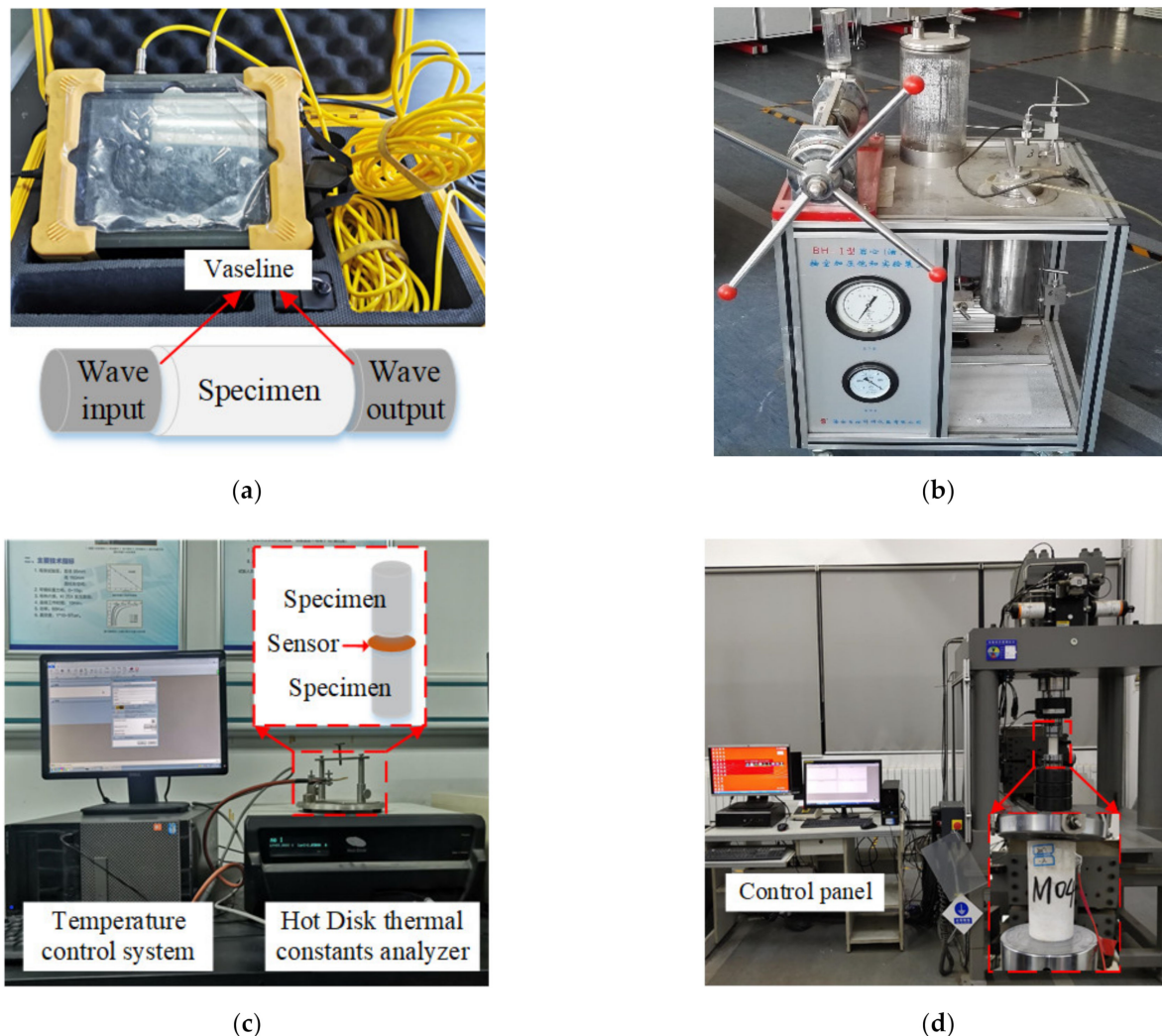


**Figure 3.** The images of (a) HC-U81 ultrasonic wave tester, (b) BH-1 rock porosity test system, (c) Hot Disk thermal constants analyzer and (d) MTS 816 servo-controlled rock mechanics test system.

Finally, uniaxial compression tests were conducted on marble specimens using the MTS 816 servo-controlled rock mechanics test system (Figure 3d). This system is capable of axial loads up to 1459 kN and strokes up to 100 mm. The constant displacement axial loading pattern of this system was selected, and the loading rate was set at 0.12 mm/min. The axial force and displacement were simultaneously recorded by the testing system during the loading process.

### 3. Analysis of Experimental Results

#### 3.1. Effects of Thermal Shock Numbers

The evolution process of the physical properties of marble specimens with the increase in thermal shock numbers is shown in Figure 4. Generally, the mass loss coefficient, volume expansion level and porosity increase with the growth of thermal shock numbers, while density, P-wave velocity and thermal conductivity gradually decrease. When  $T = 200$  and  $400$  °C, the increasing rates of mass loss and volume versus thermal shock number are minor. When  $T = 600$  °C, however, the curves of mass loss and volume with thermal shock

number show a clear increase. The mass loss coefficient and volume expansion level of a marble specimen after five thermal shocks are approximately 8.44 times and 1.79 times those after one thermal shock, respectively, as  $T = 600\text{ }^{\circ}\text{C}$ . This indicates that the exfoliation and expansion of grains become dramatic with the increase in thermal shock numbers when the heating temperature reaches  $600\text{ }^{\circ}\text{C}$ . Additionally, the variations in density show a strong correlation with mass loss and volume expansion. Density decreases by less than  $0.03\text{ g/cm}^3$  with increasing thermal shock numbers when  $T = 200$  and  $400\text{ }^{\circ}\text{C}$ , and by 4.6% at  $600\text{ }^{\circ}\text{C}$ , from  $2.77$  to  $2.67\text{ g/cm}^3$ .

During the propagation of a wave, the micro-cracks and void space inside the rock lead to the obvious refraction, diffraction and reflection of wave signals [37,38]. Therefore, P-wave velocity can be used as a useful monitoring method to detect the inside damage of rocks. When the heating temperature is between  $200$  and  $400\text{ }^{\circ}\text{C}$ , the P-wave velocity gradually decreases as the thermal shock number increases. When the thermal shock number is increased from one to five, the P-wave velocity drops from  $1.19$  to  $0.29\text{ km/s}$  with a stable decreasing rate, indicating that the marble rocks are continuously subjected to the thermal damage caused by cyclic thermal shocks. When  $T = 200$  and  $400\text{ }^{\circ}\text{C}$ , the decrease in P-wave velocity is slight as the thermal shock numbers increase. When  $T = 600\text{ }^{\circ}\text{C}$ , a continuous reduction can be observed in P-wave velocity with the increase in thermal shock numbers. This indicates that P-wave velocity is more sensitive to temperature than the cyclic thermal shock number below  $600\text{ }^{\circ}\text{C}$ .

The initial porosity ( $\phi_0$ ) of tested marble is 0.19%, suggesting the marble rocks have a tightly cemented crystal structure in their natural state. From Figure 4e, it is found that the curves of porosity versus the thermal shock number are nearly linear, and the slopes become sharper with the increase in temperature. From one to nine thermal shocks, the porosity increases by 75.68% ( $200\text{ }^{\circ}\text{C}$ ) and 68.18% ( $400\text{ }^{\circ}\text{C}$ ), respectively. At  $T = 600\text{ }^{\circ}\text{C}$ , the porosity rises from 2.48 to 5.22% when the thermal shock number increases from one to five. As a whole, similar development trends appear in the volume expansion level and porosity.

In a fire hazard, the temperature inside the rock is often uneven due to the varying distance from the fire source. Due to the influence of thermal conductivity, there is a temperature gradient inside the rock, which will induce the generation of micro-cracks. It is of great significance for the rescue efforts to study the thermal conductivity of rocks under different thermal shock numbers and temperature levels. The thermal conductivity ( $K_0$ ) of tested marble is  $4.31\text{ W/mK}$  in its natural state. As  $T = 200\text{ }^{\circ}\text{C}$ , the thermal conductivity is hardly affected by the thermal shock numbers before five thermal shocks and does not attenuate until the marble specimen undergoes seven thermal shocks. Thermal conductivity at  $T = 400$  and  $600\text{ }^{\circ}\text{C}$  decreases steadily before five thermal shocks. Previous studies have shown that the thermal conductivity of rocks is not only affected by the composition of the minerals, the size of the mineral particles, the structure of the rocks, as well as the density and humidity, but also the change in temperature [39–42]. After the cyclic thermal shock treatment, the internal structure of the rock is destroyed by high temperatures and rapid cooling, and the density and mineral composition have also changed accordingly. Therefore, as the number of cyclic thermal shocks increases, the thermal conductivity of the marble continues to decrease.

The variations of compressive strength and Young's modulus, which are the two most universal mechanical parameters, are shown in Figure 5. With the increase in thermal shock numbers, the compressive strength of the material decreases slightly. While at  $T = 400\text{ }^{\circ}\text{C}$ , the compressive strength and Young's modulus obviously decrease from one to three thermal shocks. Figure 6 displays the ultimate failure patterns of marble specimens that have experienced different cyclic thermal shocks. Three typical failure modes (axial splitting, multiple fracturing and shearing failure) and the corresponding compressive strength of the marble specimen are marked on the photos. It is found that the failure modes of the marble specimens that have been subjected to low thermal shock numbers are axial splitting and multiple fracturing when  $T = 200$  and  $400\text{ }^{\circ}\text{C}$ . With the increase in thermal shock numbers, apparent shear cracks appear on the specimen surface. Additionally,

several shear cracks with different planes appear on the surface of the specimen after nine cyclic thermal shocks of 200 °C and the specimen skin is separated from the inside rock. Marble specimens suffered further serious damage at  $T = 600\text{ °C}$ , and there is spalling of rock blocks as the thermal shock number increases.

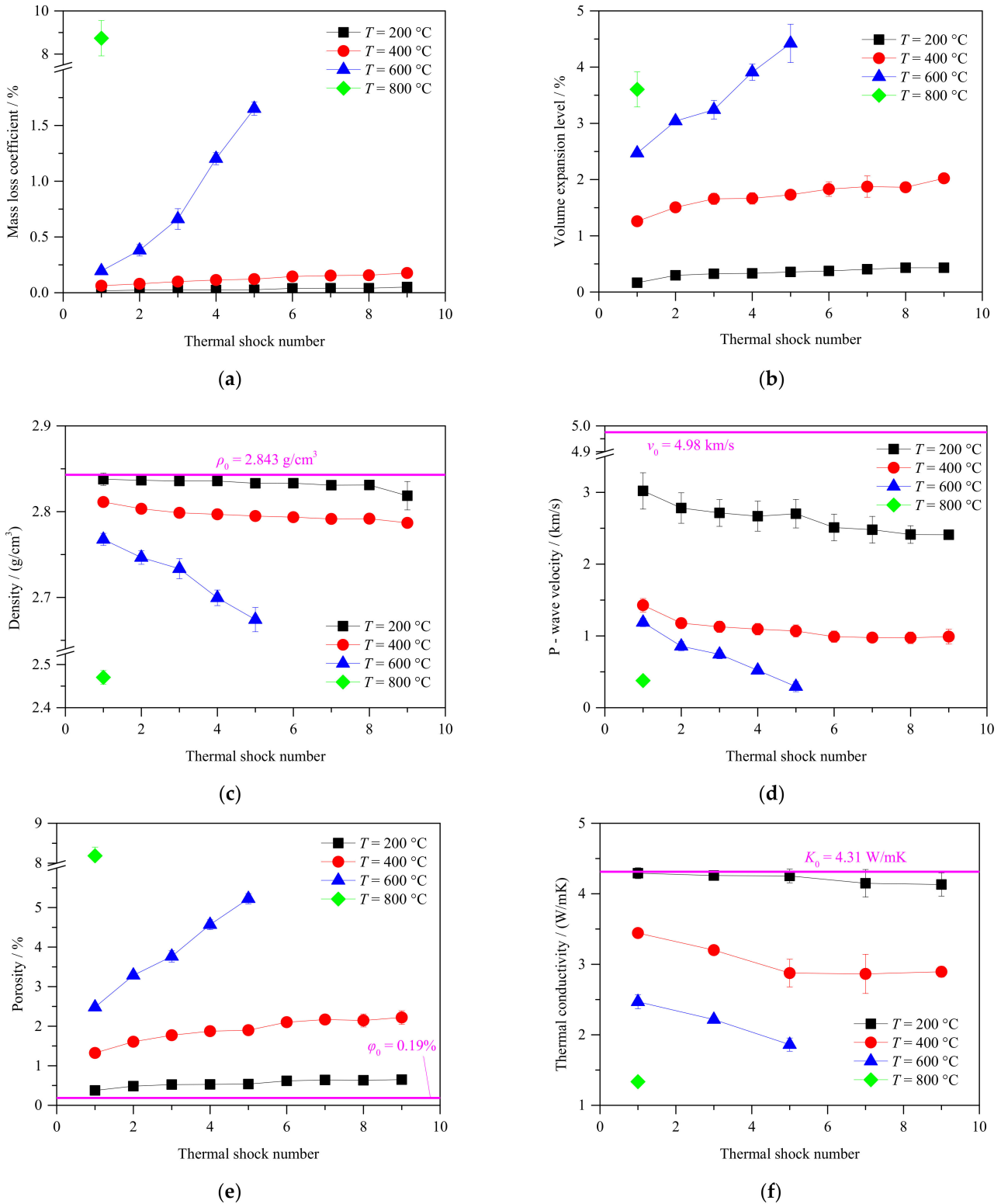


**Figure 4.** Effect of thermal shock numbers on the (a) mass loss coefficient, (b) volume expansion level, (c) density, (d) P-wave velocity, (e) porosity and (f) thermal conductivity (The error bar represents the standard deviation).

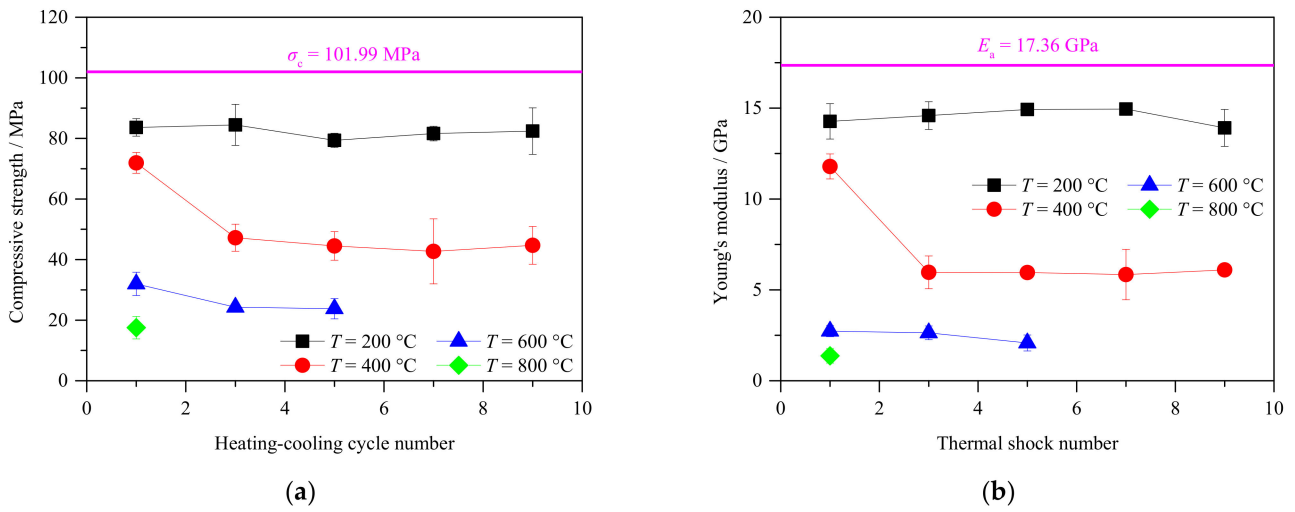


**Figure 5.** Influence of thermal shock numbers on the (a) compressive strength and (b) Young's modulus (The error bar represents the standard deviation).

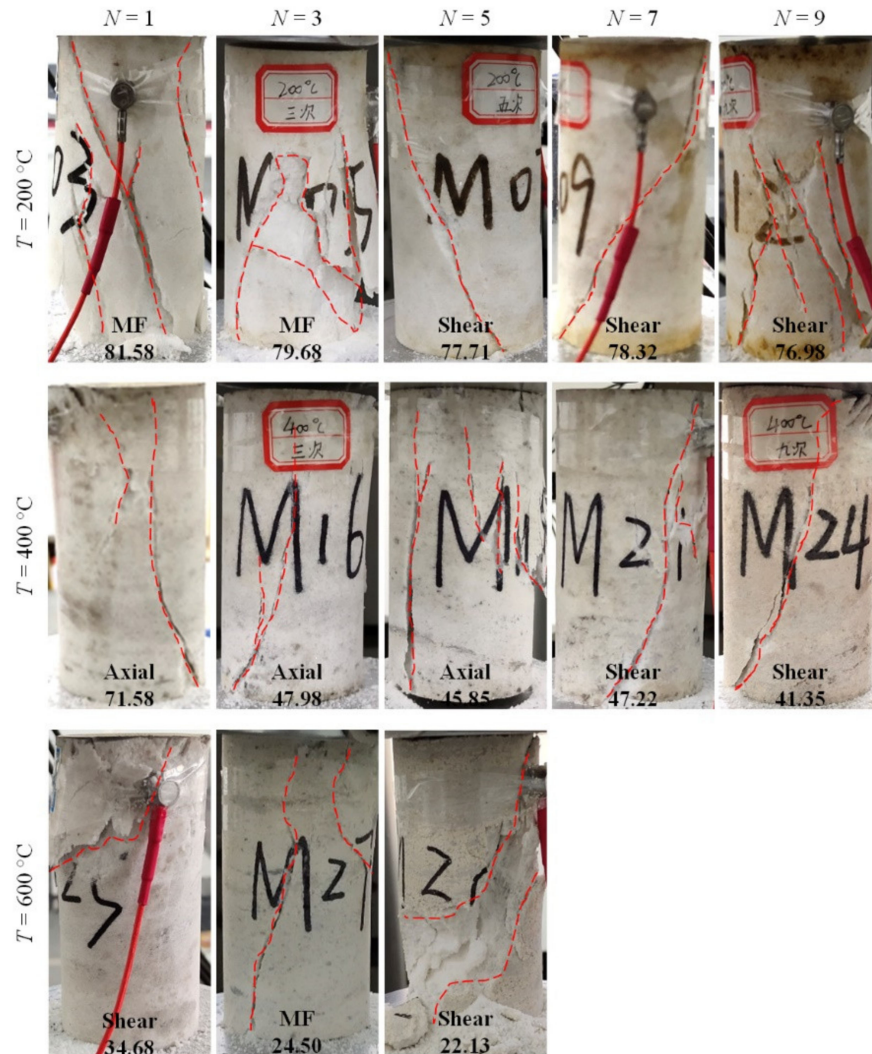


**Figure 6.** Ultimate failure modes for marble specimens at different thermal shock numbers. Failure modes and corresponding compressive strength (in MPa) are marked. (Axial denotes axial splitting, MF denotes multiple fracturing, Shear denotes shearing failure).

### 3.2. Effects of Temperature Level

The variations in the physical parameters of marble specimens after thermal shock treatment versus different temperature levels are illustrated in Figure 7. The mass loss coefficient and volume expansion level increase persistently with temperature. For the marble specimens subjected to one thermal shock, the volume expansion level increases linearly with temperature, while there is a sharp increase from 0.20 to 8.73% in the mass loss coefficient from 600 to 800 °C, respectively. Consequently, the density gradually decreases slightly in the range of 200 to 600 °C but decreases dramatically at  $T = 800$  °C. It implies that mineral decomposition and particle shedding occur at temperatures between 600 and 800 °C. In addition, an interesting phenomenon is that the thermal shock numbers affect the mass loss coefficient more obviously than the temperature level does between 400 and 600 °C. As a whole, the laws of mass, volume and density shown in marble rocks are in agreement with the results obtained in other studies [31,43].

The evolution of P-wave velocity with temperature is displayed in Figure 7d. The P-wave velocity drops sharply by nearly 50% from 200 to 400 °C and continues to fall to 0.378 km/s when the temperature reaches 800 °C. It indicates that the elevated temperature aggravates the appearance of new micro-cracks and the propagation of preexisting micro-cracks [35,44]. Cyclic thermal shock treatment on marble specimens would decrease the intergranular adhesion and generate micro-cracks, even small holes, which impedes the propagation of waves, resulting in a decrease in P-wave velocity. From 200 to 400 °C, the loss of combined and mineral water leads to the generation of pores inside the sample, which promotes the development of micro-cracks. This could explain the significant decrease in P-wave velocity in the 200–400 °C range. When the temperature reaches 600 °C, the decomposition of minerals may cause the further development of micro cracks and lead to serious thermal damage inside rocks.

Figure 7e demonstrates the variations in porosity versus temperature. After one thermal shock, the porosity in marble specimens increases steadily from 0.37 to 2.48% during the temperature range of 200–600 °C. From 600 to 800 °C, there is a noticeable increase in porosity of 5.70%, indicating that the volume and quantity of inner pores of specimens have grown significantly. The inner structural modifications caused by cyclic thermal shocks are pronounced after 600 °C, primarily due to the enlargement of preexisting micro-cracks and/or the nucleation of new micro-cracks [45]. In addition, CO<sub>2</sub> is released with the decomposition of dolomite [46], leading to structural deterioration and the generation of internal pores in rock.

The changes in thermal conductivity with the increase in temperature are shown in Figure 7f. Thermal conductivity has a generally linear relationship with temperature under the same thermal shock number. It is worth noting that the heating temperature of 200 °C has little influence on the thermal conductivity of the results, while the thermal conductivity of specimens subjected to a single thermal shock decreases linearly by 68.99% from 4.29 to 1.33 W/mK between 200 and 800 °C, indicating that increasing the temperature has a significant influence on the internal structure of marble specimens.

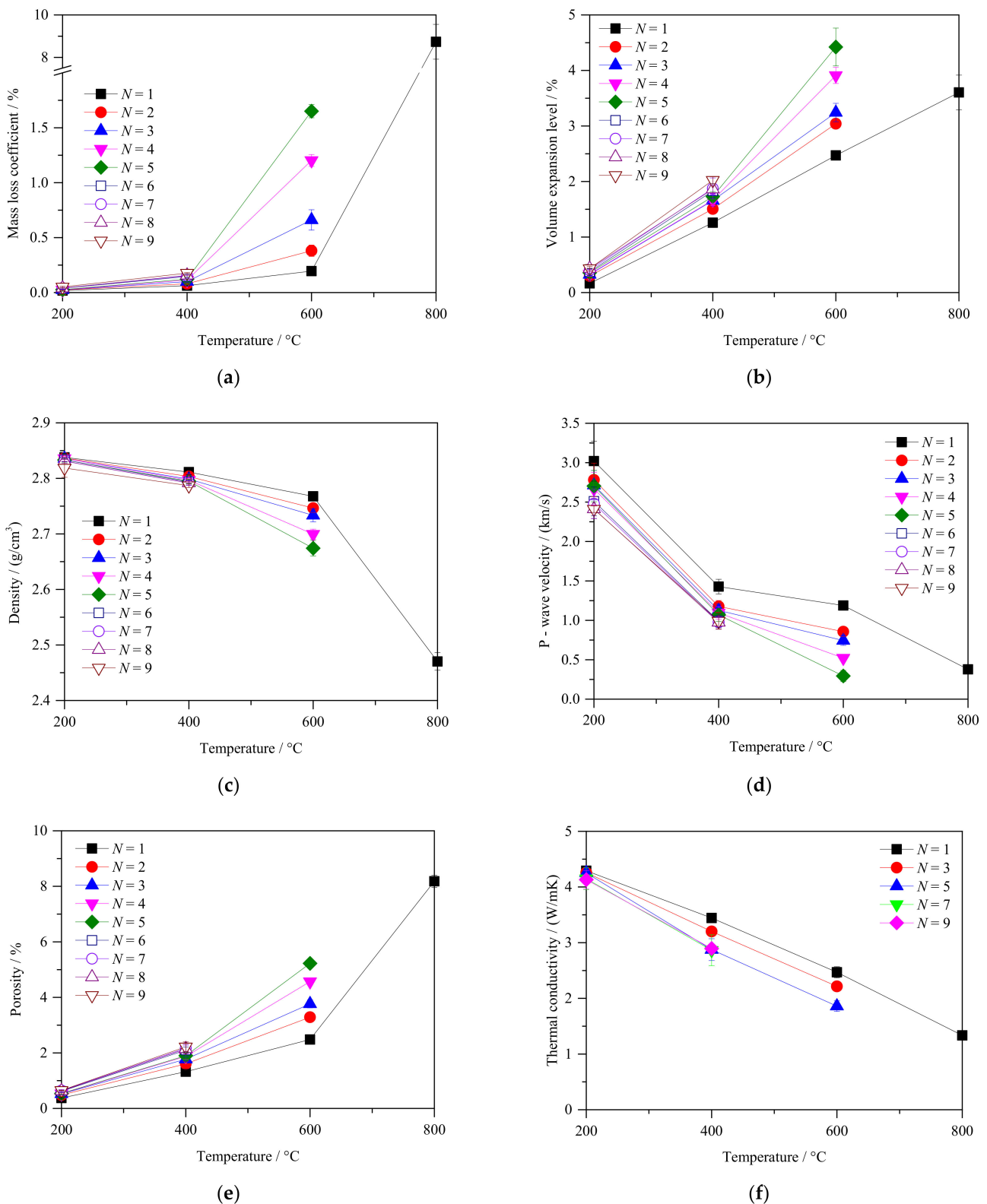


**Figure 7.** Effect of temperature levels on the (a) mass loss coefficient, (b) volume expansion level, (c) density, (d) P-wave velocity, (e) porosity and (f) thermal conductivity (The error bar represents the standard deviation).

The variations in mechanical properties, including compressive strength and Young’s modulus, are displayed in Figure 8. The compressive strength and Young’s modulus for the specimens that underwent only one thermal shock undergo a continuous decrement from

83.62 to 17.52 MPa and from 14.27 to 1.37 GPa, respectively, with the rise of the temperature from 200 to 800 °C. Micro-cracks and holes inside the rock lead to the decrement in intergranular adhesion and then result in the decrement of the bearing capacity and compressive strength of the rock. In addition, the minerals inside marble decompose and its bearing capacity weakens under high temperatures, resulting in the degeneration of the compressive strength of the whole rock [43]. The ultimate failure modes of the marble specimens that underwent thermal shocks of different temperature levels are shown in Figure 9. With the increase in temperature, in addition to the obvious decrease in compressive strength, it can be found that the main types of cracks at failure are tensile cracks and shear cracks. For specimens at room temperature ( $T = 25\text{ °C}$ ), several main tensile failure surfaces run through the whole specimen height, but the cracks are not very straight due to the presence of some large grain crystals. Due to the significant initial thermal damage, many cracks were generated and propagated under low stress levels in specimens treated with thermal shocks of 600 and 800 °C. An obvious shear surface was formed, accompanied by some clusters of minor tensile cracks, resulting in the large volumetric deformation of marble specimens.

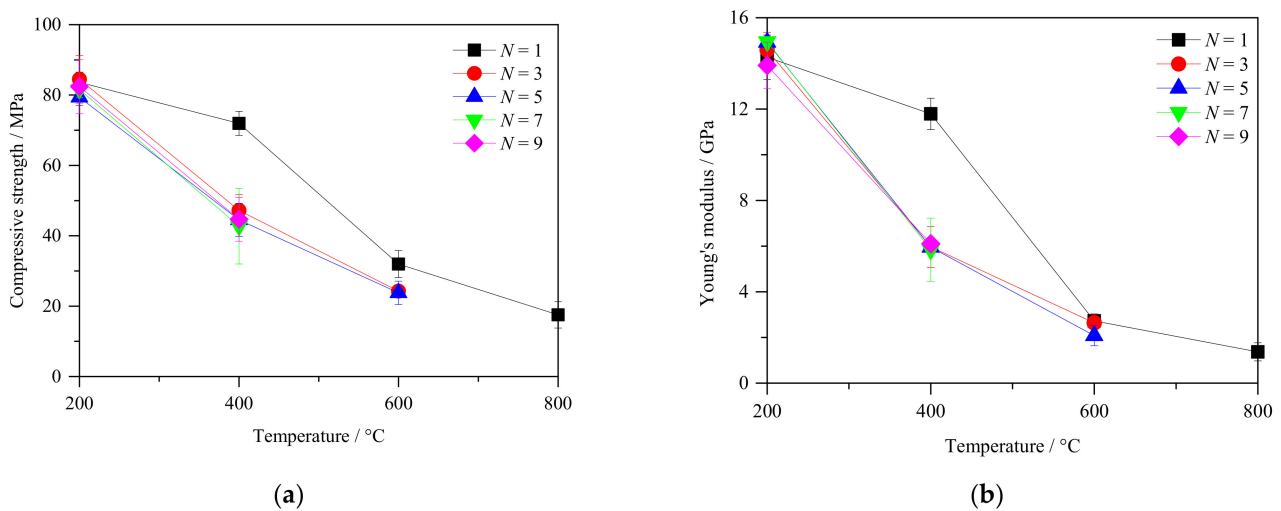


Figure 8. Influence of temperature levels on the (a) compressive strength and (b) Young’s modulus (The error bar represents the standard deviation).

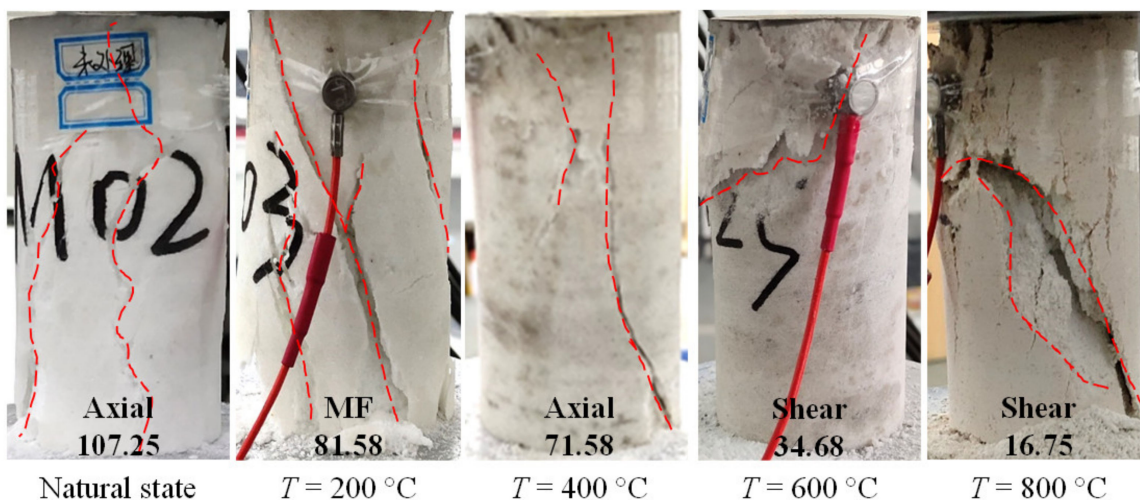
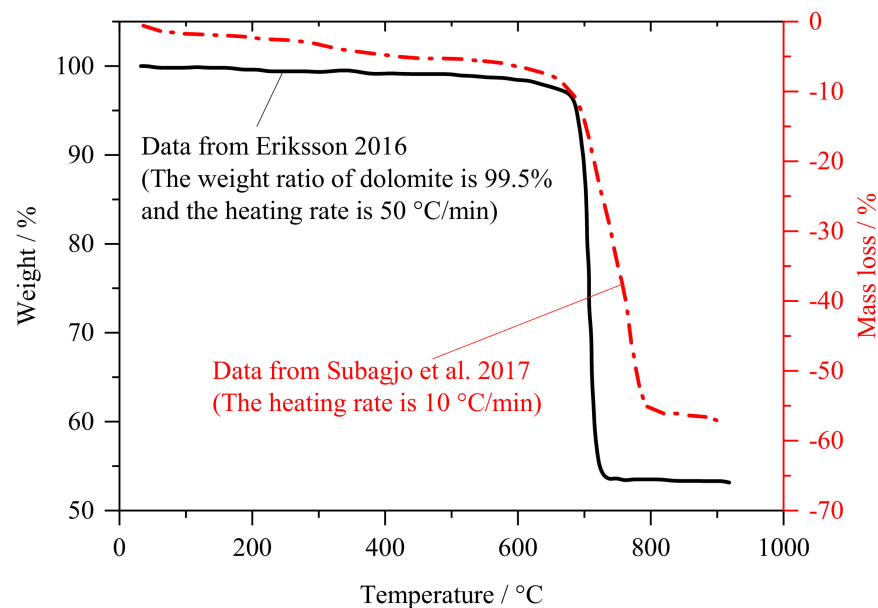
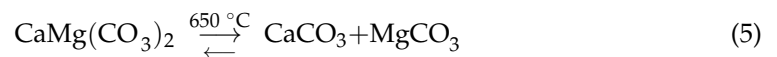
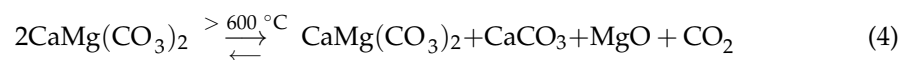


Figure 9. Ultimate failure modes for marble specimens at different temperature levels. Failure modes and corresponding compressive strength (in MPa) are marked. (Axial denotes axial splitting, MF denotes multiple fracturing, Shear denotes shearing failure).

#### 4. Micro Thermal Damage Mechanism of Marbles

##### 4.1. Thermogravimetry Analysis

To further investigate the mineral composition transformation of marble specimens, the thermogravimetry data of dolomite, the main mineral of the tested marbles, are collected from the previous literatures [47,48] and plotted in Figure 10. Dolomite is sensitive to temperature when it is subjected to the reaction temperature intervals. It can be observed that the weight of dolomite decreases slightly before 600 °C but experiences an abrupt reduction in the range of 600–800 °C. It can be implied that the dramatic thermal decomposition of dolomite from 600 to 800 °C led to the sharp decrease in mass. Dolomite will decompose into calcium carbonate, magnesium calcite and magnesium oxide at a temperature above 600 °C, as indicated in Equation (4). Then, at around 650 °C, two carbonates are formed (Equation (5)). At 700 °C, dolomite will decompose into magnesium oxide and calcium oxide, accompanied by the release of large amounts of CO<sub>2</sub> gas (Equation (6)). All the above chemical reactions are endothermic.



**Figure 10.** The thermogravimetry curves of dolomite.

##### 4.2. Microscopy Observation

The thermal damage not only results from the chemical reaction of minerals, but also is influenced by the physical changes, including crystal expansion and crystal phase transition. High temperatures result in the development of new micro-cracks, the growth of preexisting micro-cracks and the softening of the internal structure [35]. The continuous development of micro-cracks leads to the thermal damage of the internal structures of rocks, thereby weakening their strength and deformation behaviors. Therefore, microscopic observation was conducted on the marble specimens after cyclic thermal shocks using an electron microscope. The microscopic features of the marble specimens under different thermal shock conditions are exhibited in Figure 11. In order to facilitate the comparison and analysis of diversity, the same scale was selected for all the images.

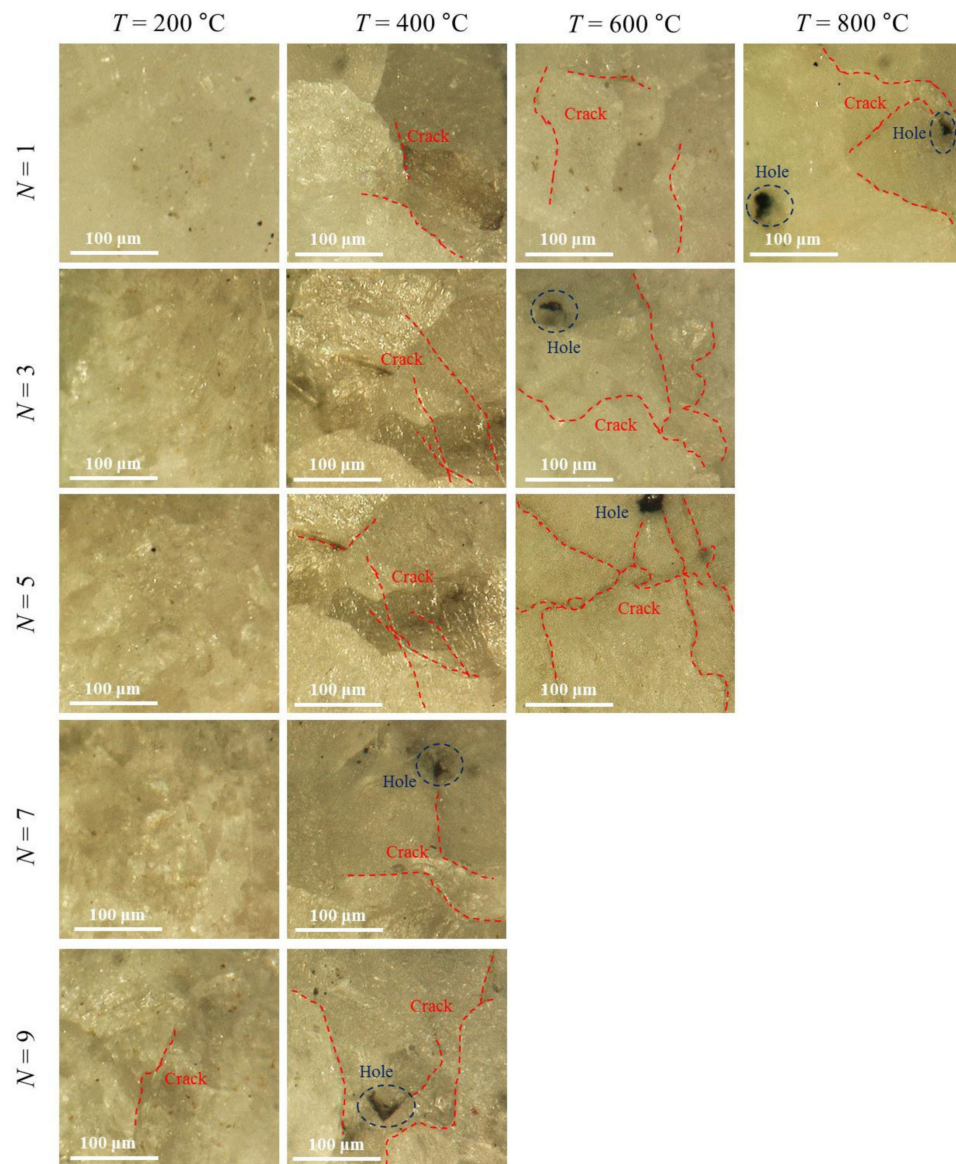


**Figure 11.** Microscopic thermal cracking feature of marble.

When marble specimens are heated to 200 °C, for  $N = 1$ , the surface morphology is smooth without obvious micro-cracks or other defects. At 200 °C, the absorbed water and combined water will continuously escape as the cyclic thermal shock number increases [8]. Due to the different thermal expansion coefficients and anisotropy of different mineral particles, a local thermal stress concentration will be caused between the mineral particles [29,49,50]. Therefore, both the flatness and smoothness of the surface topography are affected owing to the loss of water and the anisotropy thermal expansion of mineral particles. Until the thermal shock number reaches nine, micro-cracks appear on the surface.

When  $T = 400$  °C, the cementation between crystals is weakened and the boundaries between different crystals become clearly visible. The thermal expansion of crystals leads to disharmonious deformation among the mineral particles, resulting in grain separation and long-narrow intergranular cracks at grain boundaries. For  $N = 7$  and 9, the cementation between mineral particles is further weakened and small holes begin to appear on the surface. The cracks have a tendency to extend to the hole.

When  $T = 600$  °C and  $N = 1$ , the length of micro-cracks increases and the boundary between the crystals becomes blurred. For  $N = 3$ , the propagation and coalescence of microcracks become obvious and a small hole appears. For  $N = 5$ , the rock matrix was thermally decomposed into small blocks by the connected cracks, and the size of the hole

became bigger. A network of cracks appeared on the rock surface, indicating that it had experienced severe thermal damage.

After only one thermal shock at  $T = 800\text{ }^{\circ}\text{C}$ , the marble specimens show significant damage, including large cracks and holes. The boundary between the crystals is almost indistinct, indicating the melting of rock crystals at a high temperature.

According to the above analysis, microscopic cracks and the accumulation of thermal damage gradually develop with the increase in  $T$  or  $N$ , because cyclic thermal shocks induce the thermal decomposition of minerals and the expansion and melting of crystals. The structure of marble specimens gradually changes to a loosening state and cracks network inside the rocks. As a result, macroscopic cracks of rocks appear on the specimen surface (Figure 2b) and the bearing capacity is distinctly reduced.

## 5. Conclusions

In this study, the physical, mechanical and thermal cracking properties of white marble specimens that underwent cyclic thermal shocks in the temperature range of 200–800 °C were investigated experimentally. The following conclusions may be drawn:

- Both the cyclic thermal shock numbers ( $N$ ) and the temperature level ( $T$ ) have negative impacts on the physical and mechanical properties. The effect of thermal shock numbers on rock physical properties becomes dramatic as  $T = 600\text{ }^{\circ}\text{C}$ . The mass loss coefficient and porosity increase significantly from 600 to 800 °C, while the density decreases significantly. The most noticeable change in P-wave velocity occurs between 200 and 400 °C, with an attenuation of 52.98%. At  $T = 600\text{ }^{\circ}\text{C}$ , the evolutions of mass, volume and porosity show approximately linear relationships with increasing thermal shock numbers.
- The thermal conductivity of marble decreases linearly with an increasing temperature under the same thermal shock number. As  $T = 200\text{ }^{\circ}\text{C}$ , increasing the number of thermal shocks has little effect on the thermal conductivity. When  $T = 400$  and  $600\text{ }^{\circ}\text{C}$ , the thermal conductivity gradually decreases with thermal shock numbers, but the decreasing range is within 25%.
- Overall, the compressive strength and Young's modulus of the specimens vary greatly from one to three thermal shocks and then tend to be stable. While increasing temperatures constantly deteriorate the mechanical properties of marble specimens, after experiencing severe thermal damage (high  $N$  or  $T$ ), the failure mode of marble samples under uniaxial compression is mainly shear failure.
- The thermal damage induced by cyclic thermal shocks not only results from the decomposition of minerals, but is also influenced by the changes in crystal structures. Microscopic photos display the development of micro-cracks and the intensification of thermal damages with an increasing  $T$  or  $N$ .

**Author Contributions:** Methodology, H.S.; Investigation, Y.N. and Y.F.; Formal analysis, H.S., Y.F. and Y.N.; Writing—original draft, H.S. and Y.F.; Funding acquisition, H.S.; Writing—review and editing, Y.F. and H.Z. All authors have read and agreed to the published version of the manuscript.

**Funding:** This research was funded by the National Natural Science Foundation of China (No. 42077240), and Graduate Research and Innovation Projects of Jiangsu Province (KYCX21\_2279).

**Data Availability Statement:** The data that support the findings of this study are available from the corresponding author upon reasonable request.

**Conflicts of Interest:** The authors declare no conflict of interest.

## References

1. Salama, A.; El Amin, M.F.; Sun, S. Numerical investigation of high level nuclear waste disposal in deep anisotropic geologic repositories. *Prog. Nucl. Energy* **2015**, *85*, 747–755. [[CrossRef](#)]
2. Zhu, Z.-N.; Tian, H.; Jiang, G.-S.; Cheng, W. Effects of high temperature on the mechanical properties of chinese marble. *Rock Mech. Rock Eng.* **2018**, *51*, 1937–1942. [[CrossRef](#)]

3. Rong, G.; Peng, J.; Cai, M.; Yao, M.; Zhou, C.; Sha, S. Experimental investigation of thermal cycling effect on physical and mechanical properties of bedrocks in geothermal fields. *Appl. Therm. Eng.* **2018**, *141*, 174–185. [[CrossRef](#)]
4. Huang, Z.; Zeng, W.; Gu, Q.; Wu, Y.; Zhong, W.; Zhao, K. Investigations of variations in physical and mechanical properties of granite, sandstone, and marble after temperature and acid solution treatments. *Constr. Build. Mater.* **2021**, *307*, 124943. [[CrossRef](#)]
5. Krzemień, A. Fire risk prevention in underground coal gasification (UCG) within active mines: Temperature forecast by means of MARS models. *Energy* **2019**, *170*, 777–790. [[CrossRef](#)]
6. Zhao, Y.; Zhang, C.; Wang, Y.; Lin, H. Shear-related roughness classification and strength model of natural rock joint based on fuzzy comprehensive evaluation. *Int. J. Rock Mech. Min. Sci.* **2020**, *137*, 104550. [[CrossRef](#)]
7. Zhao, Y.; Liu, Q.; Zhang, C.; Liao, J.; Lin, H.; Wang, Y. Coupled seepage-damage effect in fractured rock masses: Model development and a case study. *Int. J. Rock Mech. Min. Sci.* **2021**, *144*, 104822. [[CrossRef](#)]
8. Zhang, W.; Qian, H.; Sun, Q.; Chen, Y. Experimental study of the effect of high temperature on primary wave velocity and microstructure of limestone. *Environ. Earth Sci.* **2015**, *74*, 5739–5748. [[CrossRef](#)]
9. Yin, Q.; Jing, H.; Liu, R.; Su, H.; Yu, L.; Han, G. Pore characteristics and nonlinear flow behaviors of granite exposed to high temperature. *Bull. Eng. Geol. Environ.* **2019**, *79*, 1239–1257. [[CrossRef](#)]
10. Rossi, E.; Kant, M.A.; Madonna, C.; Saar, M.O.; von Rohr, P.R. The effects of high heating rate and high temperature on the rock strength: Feasibility study of a thermally assisted drilling method. *Rock Mech. Rock Eng.* **2018**, *51*, 2957–2964. [[CrossRef](#)]
11. Yu, L.; Su, H.; Jing, H.; Zhang, Q.; Yang, E. Experimental study of the mechanical behavior of sandstone affected by blasting. *Int. J. Rock Mech. Min. Sci.* **2017**, *93*, 234–241. [[CrossRef](#)]
12. Chen, G.; Li, T.; Zhang, G.; Yin, H.; Zhang, H. Temperature effect of rock burst for hard rock in deep-buried tunnel. *Nat. Hazards* **2014**, *72*, 915–926. [[CrossRef](#)]
13. Kang, F.; Jia, T.; Li, Y.; Deng, J.; Tang, C.; Huang, X. Experimental study on the physical and mechanical variations of hot granite under different cooling treatments. *Renew. Energy* **2021**, *179*, 1316–1328. [[CrossRef](#)]
14. Qiao, R.; Shao, Z.S.; Liu, F.Y.; Wei, W. Damage evolution and safety assessment of tunnel lining subjected to long-duration fire. *Tunn. Undergr. Space Technol.* **2019**, *83*, 354–363. [[CrossRef](#)]
15. Tomar, M.S.; Khurana, S. Impact of passive fire protection on heat release rates in road tunnel fire: A review. *Tunn. Undergr. Space Technol.* **2019**, *85*, 149–159. [[CrossRef](#)]
16. Shao, S.; Ranjith, P.G.; Wasantha, P.L.P.; Chen, B.K. Experimental and numerical studies on the mechanical behaviour of Australian Strathbogie granite at high temperatures, An application to geothermal energy. *Geothermics* **2015**, *54*, 96–108. [[CrossRef](#)]
17. Peng, J.; Rong, G.; Tang, Z.; Sha, S. Microscopic characterization of microcrack development in marble after cyclic treatment with high temperature. *Bull. Eng. Geol. Environ.* **2019**, *78*, 5965–5976. [[CrossRef](#)]
18. Feng, Y.; Su, H.; Zhang, W.; Yu, L.; Yin, Q. Experimental study on mechanical behaviors and fracture features of coarse marble specimens after thermal shock. *Int. J. Geomech.* **2021**, *21*, 06021013. [[CrossRef](#)]
19. Guo, Q.; Su, H.; Liu, J.; Yin, Q.; Jing, H.; Yu, L. An experimental study on the fracture behaviors of marble specimens subjected to high temperature treatment. *Eng. Fract. Mech.* **2020**, *225*, 106862. [[CrossRef](#)]
20. Zhao, Y.; Zhang, L.; Liao, J.; Wang, W.; Liu, Q.; Tang, L. Experimental study of fracture toughness and subcritical crack growth of three rocks under different environments. *Int. J. Geomech.* **2020**, *20*, 04020128. [[CrossRef](#)]
21. Koca, M.Y.; Ozden, G.; Yavuz, A.B.; Kincal, C.; Onargan, T.; Kucuk, K. Changes in the engineering properties of marble in fire-exposed columns. *Int. J. Rock Mech. Min. Sci.* **2006**, *43*, 520–530. [[CrossRef](#)]
22. Xu, G.; Sun, H.L.; Li, S.C. Research on the Ecological Scheduling Decisions of the Jinping Cascade Hydropower Station on the Yalong River. *Energy Sources Part A* **2014**, *36*, 1115–1122. [[CrossRef](#)]
23. Gong, M.; Qi, S.; Liu, J. Engineering geological problems related to high geo-stresses at the Jinping I Hydropower Station, Southwest China. *Bull. Eng. Geol. Environ.* **2010**, *69*, 373–380. [[CrossRef](#)]
24. Zhao, J.; Feng, X.-T.; Zhang, X.-W.; Zhang, Y.; Zhou, Y.-Y.; Yang, C.-X. Brittle-ductile transition and failure mechanism of Jinping marble under true triaxial compression. *Eng. Geol.* **2018**, *232*, 160–170. [[CrossRef](#)]
25. Zhu, G.-Q.; Feng, X.-T.; Zhou, Y.-Y.; Li, Z.-W.; Yang, C.-X.; Gao, Y.-H. Experimental study to design an analog material for Jinping marble with high strength, high brittleness and high unit weight and ductility. *Rock Mech. Rock Eng.* **2019**, *52*, 2279–2292. [[CrossRef](#)]
26. Gautam, P.K.; Jha, M.K.; Verma, A.K.; Singh, T.N. Experimental study of thermal damage under compression and tension of Makrana marble. *J. Therm. Anal. Calorim.* **2020**, *139*, 609–627. [[CrossRef](#)]
27. Zhang, Y.L.; Sun, Q.; Geng, J.S. Microstructural characterization of limestone exposed to heat with XRD, SEM and TG-DSC. *Mater. Charact.* **2017**, *134*, 285–295. [[CrossRef](#)]
28. Li, M.; Mao, X.B.; Cao, L.L.; Pu, H.; Lu, A.H. Influence of Heating Rate on the Dynamic Mechanical Performance of Coal Measure Rocks. *Int. J. Geomech.* **2017**, *17*, 04017020. [[CrossRef](#)]
29. Zhang, F.; Zhao, J.; Hu, D.; Skoczylas, F.; Shao, J. Laboratory Investigation on Physical and Mechanical Properties of Granite After Heating and Water-Cooling Treatment. *Rock Mech. Rock Eng.* **2018**, *51*, 677–694. [[CrossRef](#)]
30. Zhang, F.; Zhang, Y.; Yu, Y.; Hu, D.; Shao, J. Influence of cooling rate on thermal degradation of physical and mechanical properties of granite. *Int. J. Rock Mech. Min. Sci.* **2020**, *129*, 104285. [[CrossRef](#)]
31. Ozguven, A.; Ozcelik, Y. Effects of high temperature on physico-mechanical properties of Turkish natural building stones. *Eng. Geol.* **2014**, *183*, 127–136. [[CrossRef](#)]

32. Peng, J.; Rong, G.; Cai, M.; Yao, M.-D.; Zhou, C.-B. Physical and mechanical behaviors of a thermal-damaged coarse marble under uniaxial compression. *Eng. Geol.* **2016**, *200*, 88–93. [[CrossRef](#)]
33. Fairhurst, C.E.; Hudson, J.A. Draft ISRM suggested method for the complete stress–strain curve for the intact rock in uniaxial compression. *Int. J. Rock Mech. Min. Sci.* **1999**, *36*, 279–289.
34. Kumari, W.G.P.; Ranjith, P.G.; Perera, M.S.A.; Chen, B.K. Experimental investigation of quenching effect on mechanical, microstructural and flow characteristics of reservoir rocks: Thermal stimulation method for geothermal energy extraction. *J. Pet. Sci. Eng.* **2018**, *162*, 419–433. [[CrossRef](#)]
35. Zhang, W.; Sun, Q.; Hao, S.; Geng, J.; Lv, C. Experimental study on the variation of physical and mechanical properties of rock after high temperature treatment. *Appl. Therm. Eng.* **2016**, *8*, 1297–1304. [[CrossRef](#)]
36. Zhu, T.; Jing, H.; Su, H.; Yin, Q.; Du, M.; Han, G. Physical and mechanical properties of sandstone containing a single fissure after exposure to high temperatures. *Int. J. Min. Sci. Technol.* **2016**, *26*, 319–325. [[CrossRef](#)]
37. Nakao, A.; Nara, Y.; Kubo, T. P-wave propagation in dry rocks under controlled temperature and humidity. *Int. J. Rock Mech. Min. Sci.* **2016**, *86*, 157–165. [[CrossRef](#)]
38. Liu, Q.; Qian, Z.; Wu, Z. Micro/macro physical and mechanical variation of red sandstone subjected to cyclic heating and cooling: An experimental study. *Bull. Eng. Geol. Environ.* **2017**, *78*, 1485–1499. [[CrossRef](#)]
39. Miao, S.Q.; Li, H.P.; Chen, G. Temperature dependence of thermal diffusivity, specific heat capacity, and thermal conductivity for several types of rocks. *J. Therm. Anal. Calorim.* **2013**, *115*, 1057–1063. [[CrossRef](#)]
40. Tang, F.; Wang, L.; Lu, Y.; Yang, X. Thermophysical properties of coal measure strata under high temperature. *Environ. Earth Sci.* **2015**, *73*, 6009–6018. [[CrossRef](#)]
41. Kant, M.A.; Ammann, J.; Rossi, E.; Madonna, C.; Höser, D.; von Rohr, P.R. Thermal properties of Central Aare granite for temperatures up to 500 °C: Irreversible changes due to thermal crack formation. *Geophys. Res. Lett.* **2017**, *44*, 771–776. [[CrossRef](#)]
42. Sun, Q.; Zhang, W.; Zhu, Y.; Huang, Z. Effect of high temperatures on the thermal properties of granite. *Rock Mech. Rock Eng.* **2019**, *52*, 2691–2699. [[CrossRef](#)]
43. Su, H.; Jing, H.; Yin, Q.; Yu, L.; Wang, Y.; Wu, X. Strength and deformation behaviors of veined marble specimens after vacuum heat treatment under conventional triaxial compression. *Acta Mech. Sin.* **2017**, *33*, 886–898. [[CrossRef](#)]
44. Liu, S.; Xu, J. An experimental study on the physico-mechanical properties of two post-high-temperature rocks. *Eng. Geol.* **2015**, *185*, 63–70. [[CrossRef](#)]
45. Géraud, Y. Variations of connected porosity and inferred permeability in a thermally cracked granite. *Geophys. Res. Lett.* **1994**, *21*, 979–982. [[CrossRef](#)]
46. De Aza, A.H.; Rodriguez, M.A.; Rodriguez, J.L.; De Aza, S.; Pena, P.; Convert, P.; Hansen, T.; Turrillas, X. Decomposition of dolomite monitored by neutron thermodiffraction. *J. Am. Ceram. Soc.* **2002**, *85*, 881–888. [[CrossRef](#)]
47. Eriksson, M. Characterization of kiln feed limestone by dynamic heating rate thermogravimetry. *Int. J. Miner. Process.* **2016**, *147*, 31–42. [[CrossRef](#)]
48. Subagio; Wulandari, W.; Adinata, P.M.; Fajrin, A. Thermal decomposition of dolomite under CO<sub>2</sub>-air atmosphere. *AIP Conf. Proc.* **2017**, *1805*, 040006.
49. Yin, Q.; Wu, J.; Zhu, C.; Wang, Q.; Zhang, Q.; Jing, H.; Xie, J. The role of multiple heating and water cooling cycles on physical and mechanical responses of granite rocks. *Geomech. Geophys. Geo Energy Geo Resour.* **2021**, *7*, 1–26. [[CrossRef](#)]
50. Feng, G.; Kang, Y.; Chen, F.; Liu, Y.-W.; Wang, X.-C. The influence of temperatures on mixed-mode (I + II) and mode-II fracture toughness of sandstone. *Eng. Fract. Mech.* **2018**, *189*, 51–63. [[CrossRef](#)]